Compact objects physics
in the realm of multi-messenger astronomy

Diego Sáez-Chillón Gómez

From Black Holes to the Cosmos: Matt Visser's journey through space and time
24–28 de agosto de 2026 SISSA, Trieste

Universidad de Valladolid

MINISTERIO DE CIENCIA, INNOVACIÓN Y UNIVERSIDADES
Cofinanciado por la Unión Europea
AGENCIA ESTATAL DE INVESTIGACIÓN

Motivation

Classical Black Holes

- Singularity

Black bounces

- No singularities

Our aim

Can black bounces be tested observationally? (e.g., through QNMs and/or shadows)

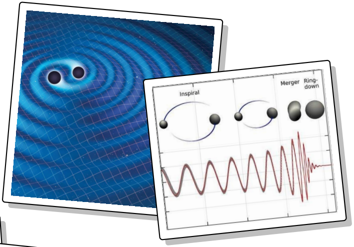

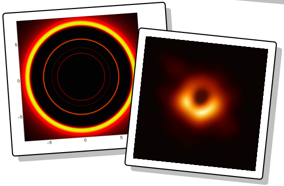

Outline

1. Black bounces
2. Ray tracing and Shadows
3. Gravitational waves: Quasinormal modes
4. Multi-messenger Astronomy

Outline

Black bounces

The most general static spherically symmetric line element can be expressed as follows

$$ds^2 = -A(r)dt^2 + \frac{dr^2}{A(r)} + \Sigma^2(r)\left(d\theta^2 + \sin\theta d\phi^2\right), \qquad (1)$$

Then, a regular asymptotically flat black bounce spacetime would hold the following conditions [1],

- For $r \to \pm\infty$, then $A(r) \to 1$ and $\Sigma(r) \to r$.
- $A(r)$ and $\Sigma(r)$ are regular everywhere $-\infty < r < \infty$.
- For $r \to 0$, then $\Sigma(0) = c_0$, $\Sigma'(0) = 0$ and $\Sigma''(0) > 0$.

[1] G. Alencar, A. Duran-Cabacés, D. Rubiera-Garcia and D. Sáez-Chillón Gómez, Phys. Rev. D **111**, no.10, 104020 (2025)

Black bounces

Simpson-Visser spacetime as an example:

$$A(r) = 1 - \frac{2M}{\sqrt{r^2 + a^2}} \quad \text{and} \quad \Sigma^2(r) = r^2 + a^2$$

. The bounce is located at $x = 0$.

- For $0 < a < 2m$, the metric represents a regular black hole.
- For $a > 2m$, the metric represents a two-way traversable wormhole.
- For $a = 2m$, the metric represents a one-way wormhole.

Black bounces

Generalized Simpson-Visser spacetime (Bardeen-like wormhole). [2]

$$A(r) = 1 - \frac{2Mr^2}{(r^2+a^2)^{3/2}} \quad ; \quad \Sigma(r) = \sqrt{r^2+a^2}. \tag{2}$$

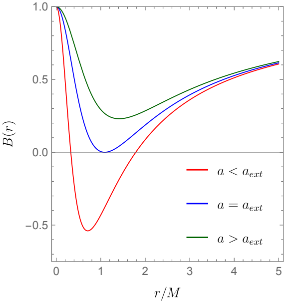

Figure 1: Radial function $B(r)$ plotted for different values of a.

The model transitions between a **regular black hole** and a **traversable wormhole** at the extreme value:

$$a_{ext} = \frac{4M}{3\sqrt{3}} \tag{3}$$

[2] F. S. N. Lobo, M. E. Rodrigues, M. V. de Sousa Silva, A. Simpson and M. Visser, Phys. Rev. D 103 (2021) 084052

Outline

1. Black bounces
2. Ray tracing and Shadows
3. Gravitational waves: Quasinormal modes
4. Multi-messenger Astronomy

Light trajectories

The equation for null geodesics is given by:

$$\dot{r}^2 = \frac{1}{b^2} - V(r) \ , \quad V(r) = \frac{A(r)}{\Sigma(r)} \ , \tag{4}$$

where the impact parameter is defined as:

$$b = \frac{L}{E} = \frac{\Sigma(r)\dot{\phi}}{A(r)\dot{t}} \ , \tag{5}$$

The equation for the trajectory leads to:

$$\frac{dr}{d\phi} = \mp \frac{b}{\Sigma^2\sqrt{1 - b^2 A/\Sigma^2}} \tag{6}$$

Hence, the photon trajectory is deflected closed to the object,

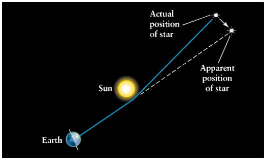

$$\alpha(b) = I(b) - \pi \ , \quad I(b) = 2\int_{r_0(b)}^{\infty} \frac{dr}{\sqrt{\frac{F(r)\Sigma(r)}{B(r)}}} \tag{7}$$

Shadows

For compact enough objects, there might be one or several circular orbits for photons, $\dot{r} = \ddot{r} = 0$. The final image is a structure of photon rings composed by photons that go directly from the accretion disk, those that are slightly lensed and those that go around the object at least once.[3]

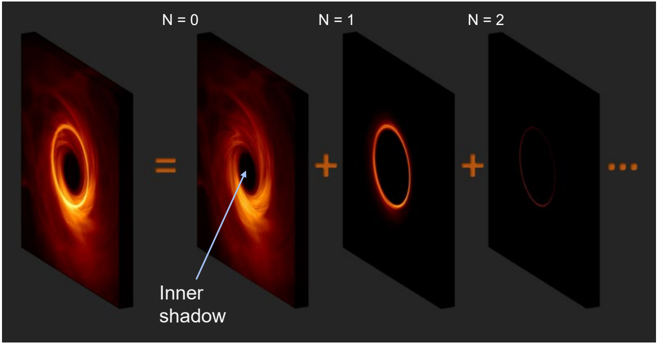

[3] Paul Tiede, On Photon-ring paper in M87* and nature of object, Black Holes in and Out, Copenhagen, 2024

Simpson-Visser spacetime

For this case, $A(r) = B^{-1}(r) = 1 - \frac{2M}{r(x)}$ and $\Sigma(r) = r(x)$, where $r(x) = \sqrt{x^2 + a^2}$. And the equation of motion can be expressed as: $\dot{x}^2 = \frac{1}{b^2} - V(x)$.

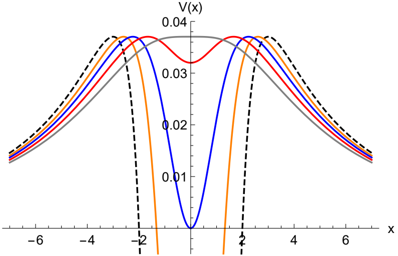

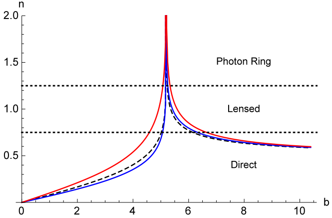

Simpson-Visser spacetime

Ray tracing

The ray tracing consists on calculating the photon trajectories from the observer screen till the central object for a continues range of the impact parameter.

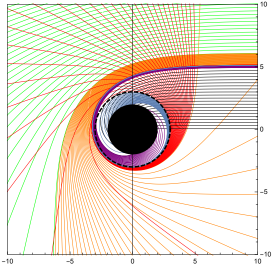

Figure 2: Schwarzschild black hole.

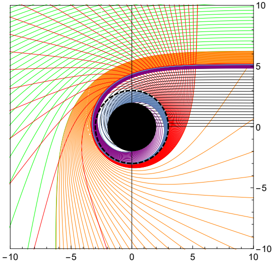

Figure 3: Regular black hole.

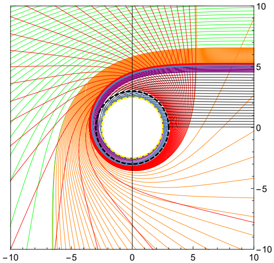

Figure 4: Wormhole.

Simpson-Visser spacetime

The result is an optical appearance that show a superposition of photon rings whose structure might vary from a class of object to another. [4]

$$I^{obs} = \sum_m A^2(x) I(x)\Big|_{x=x_m(b)} \tag{8}$$

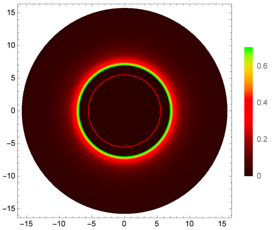

Figure 5: Schwarzschild black hole.

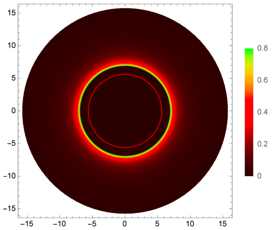

Figure 6: Regular black hole.

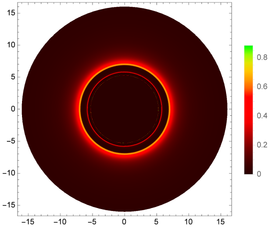

Figure 7: Wormhole.

[4] M. Guerrero, G. J. Olmo, D. Rubiera-Garcia and D. Sáez-Chillón Gómez, JCAP **08** (2021), 036

Generalized Simpson-Visser spacetime

For this case, $A(x) = B^{-1}(x) = 1 - \frac{2Mx^2}{(x^2+a^2)^{3/2}}$ and $\Sigma^2(x) = x^2 + a^2$. And the equation of motion can be expressed as: $\dot{x}^2 = \frac{1}{b^2} - V(x)$.

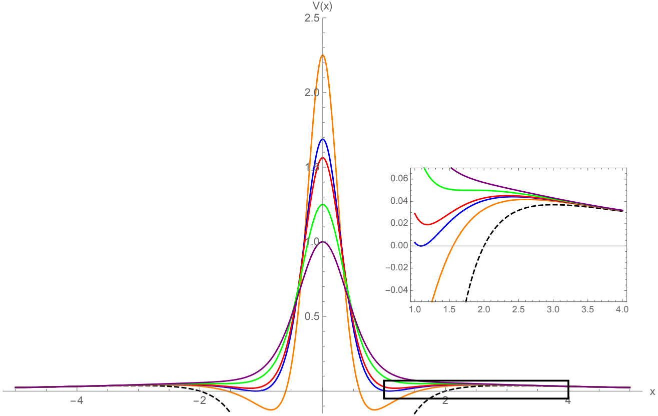

Generalized Simpson-Visser spacetime

Ray tracing

Wormhole described by the generalization of the Simpson-Visser metric with $a = 0.78M$, which shows the existence of two photon spheres.

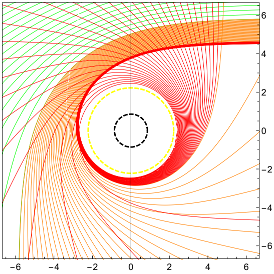

Figure 8: Outer trajectories.

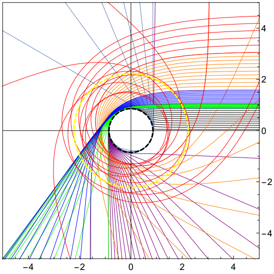

Figure 9: Inner trajectories.

Generalized Simpson-Visser spacetime

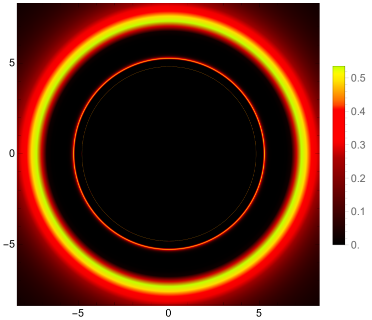

Figure 10: Images of a modified black hole with $a = 0.76M$ (left) and of a traversable wormhole with $a = 0.78M$ (right) for the generalized black bounce proposal within a SU emission profile that peaks in the vicinity of the innermost stable circular orbit of time-like observers.[5]

[5] M. Guerrero, G. J. Olmo, D. Rubiera-Garcia and D. Sáez-Chillón Gómez, Phys. Rev. D **105** (2022) no.8, 084057

Outline

Gravitational waves

Binary systems mergers

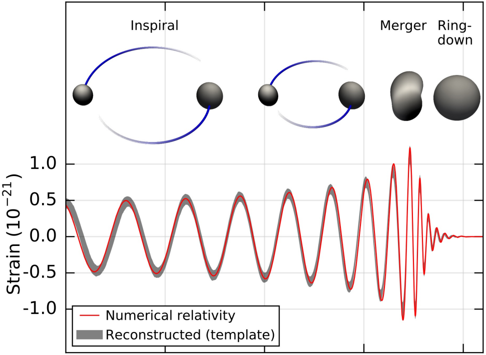

Figure 11: Phases of a binary system merger.

The ringdown can be well described by perturbation theory, which leads to a wave package described by quasinormal modes.

Quasinormal modes (QNMs)

QNMs are the vibrational response of a BH (or a compact object) to small perturbations. They are the solutions to the equation

$$\left[\partial^2_{r*} + \left(\omega^2 - V_l^{RW}(r)\right)\right] \tilde{\phi}(r, \omega) = 0, \tag{9}$$

that satisfies the following conditions

$$\tilde{\phi}(r^* \to -\infty, \omega) \sim e^{-i\omega r^*}, \quad \tilde{\phi}(r^* \to \infty, \omega) \sim e^{i\omega r^*} \ , \tag{10}$$

As a result complex frequencies are obtained,

$$\omega = \omega_R + i \cdot \omega_I. \tag{11}$$

Real part describes oscillation rate and imaginary part describes damping rate.

Quasinormal modes (QNMs)

Time-domain method

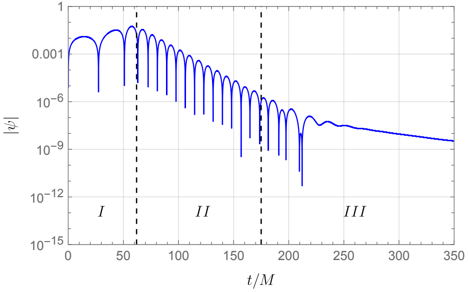

Figure 12: Time profile of a Gaussian wave packet under the potential of a RBH divided in its three main phases.

We can decompose the time profile in its vibrational modes using the Prony fitting method[6]

$$\psi(t) = \sum_{n=0}^{N} C_n e^{-i\omega_n t}. \quad (12)$$

The time profile is almost monochromatic at phase II $\Rightarrow$ fundamental mode.

Cons

Relies on numerical accuracy

Pros

Dynamical information.

[6] R. A. Konoplya and A. Zhidenko, Rev. Mod. Phys. 83 (2011) 793.

Quasinormal modes for the BB case ($a \leq a_{ext}$)[7]

By computing the **fundamental mode** for $0 \leq a \leq a_{ext}$, we find that QNMs can help distinguish RBHs from BHs. As a increases, the perturbation has

- Faster oscillation.
- Slower damping rate.

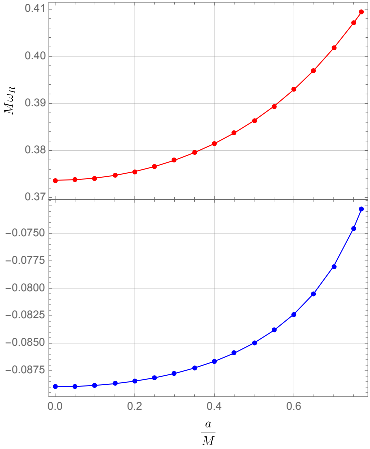

Figure 13: Real part (top, red) and imaginary part (bottom, blue) of the fundamental QNM for the RBH case, with $l = 2$.

[7] A. Duran-Cabacés, D. Rubiera-Garcia, and D. Sáez-Chillón Gómez, Phys. Rev. D 112, 044016 (2025)

Quasinormal modes for the TW case ($a > a_{ext}$)

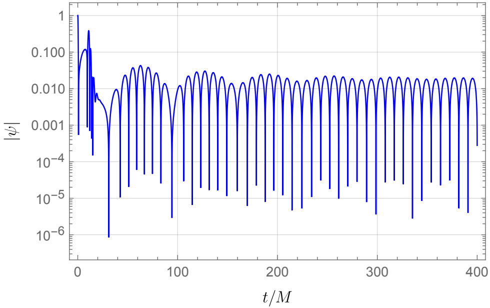

Figure 14: Time profile of a Gaussian wave packet under the potential of a TW. It can be observed that echoes emerge after the transitory phase.

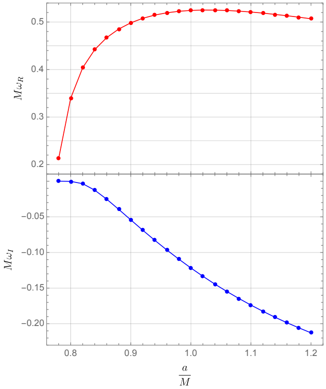

Figure 15: Real part (top, red) and imaginary part (bottom, blue) of the fundamental QNM for the TW case, with $l = 2$.

Quasinormal modes for the TW case ($a > a_{ext}$)

The echoes emerge due to the multi-peak structure of the potential. They disappear at $a \gtrsim a_{echoes} = 2\sqrt{5}/5\ M \approx 0.894\ M$

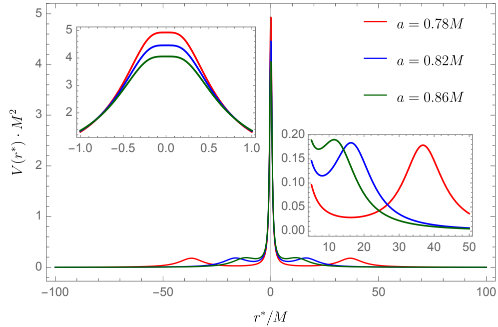

Figure 16: Potential for different values of the parameter $a > a_{ext}$. The potential well gets shallower as a increases.

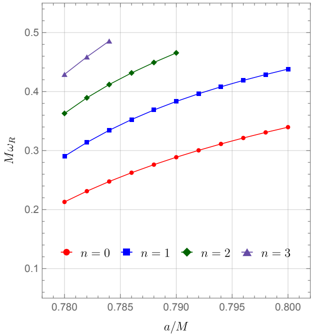

Figure 17: Real part of the measurable overtones for each value of the parameter $a > a_{ext}$.

Outline

Correspondence Shadows & Gravitational Waves

In the eikonal limit ($l >> n$), the Regge-Wheeler potential reduces to the potential followed by photons, such that we find that (in the WKB approximation)[8]:

$$\omega_R + i\omega_I \approx \left(l + \frac{1}{2}\right)\Omega_c - i\left(n + \frac{1}{2}\right)|\lambda|, \tag{13}$$

where $\Omega_c = 1/b_c$ is the angular velocity of circular orbits for photons, while $\lambda = \gamma_c/\pi b_c$ sets the principal Lyapunov exponent that characterizes the drift of radial distance in the stability of null geodesics and it is related to the demagnification of the different emissions.

Open door

Multi-messenger observational study of BHs: correlations of GWs frequencies with properties of direct images.

[8] V. Cardoso, A. S. Miranda, E. Berti, H. Witek and V. T. Zanchin, Phys. Rev. D 79 (2009) 064016.
D. Díaz-Guerra, Á. Rincón, D. Rubiera-Garcia and D. Saez-Chillon Gomez, Phys. Rev. D **114**, no.4, 044090 (2026)

Correspondence Shadows & Gravitational Waves

Model	$A(r)$	$b_{\rm ps}^{\rm BHI}$	$\gamma_{\rm ps}^{\rm BHI}$	ℓ	**QNMs** $(\omega_R + i\omega_I)$	$b_{\rm ps}^{\rm QNM}$	$b_{\rm ps}^{\rm QNM}/b_{\rm ps}^{\rm BHI}$	$\gamma_{\rm ps}^{QNM}$	$\gamma_{\rm ps}^{QNM}/\gamma_{\rm ps}^{\rm BHI}$
				10	$2.021320 - 0.096256\,i$	5.195	1.000	3.142	1.000
				8	$1.636560 - 0.096272\,i$	5.194	1.000	3.142	1.000
Schwarzschild	$1 - \frac{2M}{r}$	5.196	3.142	6	$1.251890 - 0.096310\,i$	5.192	0.999	3.142	1.000
				4	$0.867400 - 0.096390\,i$	5.188	0.998	3.142	1.000
				2	$0.484000 - 0.097000\,i$	5.165	0.994	3.148	1.002
				10	$2.494810 - 0.094645\,i$	4.209	1.000	2.503	0.990
				8	$2.019909 - 0.094653\,i$	4.208	1.000	2.503	0.990
RN	$1 - \frac{2M}{r} + \frac{q_e^2}{r^2}$	4.209	2.527	6	$1.545111 - 0.094670\,i$	4.207	0.999	2.502	0.990
$q_e = 0.939$				4	$1.070553 - 0.094714\,i$	4.203	0.999	2.501	0.990
				2	$0.596822 - 0.094905\,i$	4.189	0.995	2.498	0.988
				10	$2.321584 - 0.077895\,i$	4.523	1.000	2.214	0.983
				8	$1.879547 - 0.077908\,i$	4.522	1.000	2.214	0.983
Bardeen	$1 - \frac{2Mr^2}{(r^2+q_m^2)^{3/2}}$	4.524	2.253	6	$1.437568 - 0.077936\,i$	4.522	0.999	2.214	0.983
$q_m = 0.7698$				4	$0.995722 - 0.078008\,i$	4.519	0.999	2.214	0.983
				2	$0.554324 - 0.078332\,i$	4.510	0.997	2.220	0.985
				10	$2.135769 - 0.081463\,i$	4.916	1.000	2.516	0.990
				8	$1.729082 - 0.081466\,i$	4.916	1.000	2.516	0.990
Hayward	$1 - \frac{2Mr^2}{r^3+2l^2M}$	4.916	2.542	6	$1.322440 - 0.081474\,i$	4.913	0.999	2.516	0.990
$l = \sqrt{16/27}$				4	$0.915908 - 0.081501\,i$	4.916	1.000	2.516	0.990
				2	$0.509747 - 0.081723\,i$	4.904	0.997	2.518	0.991
				10	$2.451426 - 0.088177\,i$	4.283	1.000	2.373	0.988
				8	$1.984639 - 0.088184\,i$	4.283	1.000	2.373	0.988
Frolov	$1 - \frac{(2Mr-q_e^2)r^2}{r^4+(2Mr+q_e^2)l^2}$	4.283	2.403	6	$1.517906 - 0.088198\,i$	4.282	1.000	2.373	0.988
$q_e = 0.875$	$l = 0.3$			4	$1.051298 - 0.088236\,i$	4.280	0.999	2.373	0.988
				2	$0.585116 - 0.088429\,i$	4.273	0.998	2.374	0.988

Figure 18: Comparison of the values of the critical impact parameter and the Lyapunov exponent from direct BHI procedures, and from the analysis of massless scalar QNMs using the sixth-order WKB approximation for $n = 0$.[9]

[9] D. Díaz-Guerra, Á. Rincón, D. Rubiera-Garcia and D. Saez-Chillon Gomez, Phys. Rev. D **114**, no.4, 044090 (2026)

Thank you very much!